



INVERSION OF ULTRAFINE CONDENSATION NUCLEUS COUNTER PULSE HEIGHT DISTRIBUTIONS TO OBTAIN NANOPARTICLE ($\sim 3\text{--}10$ nm) SIZE DISTRIBUTIONS

Rodney J. Weber,^{*†} Mark R. Stolzenburg,[‡] Spyros N. Pandis[§] and Peter H. McMurry[¶]

^{*}Environmental Chemistry Division, Brookhaven National Laboratory, Building 815E, Upton, NY 11973-5000, U.S.A.

[‡]Aerosol Dynamics Inc., 2329 Fourth St., Berkeley, CA 94710, U.S.A.

[§]Department of Chemical Engineering, Carnegie Mellon University, Pittsburgh, PA 15213, U.S.A.

[¶]Particle Technology Laboratory, Department of Mechanical Engineering, 111 Church St. SE, University of Minnesota, Minneapolis, MN 55455, U.S.A.

(First received 7 April 1997; and in final form 10 October 1997)

Abstract—Previous work (Ahn and Liu (1990) *J. Aerosol. Sci.* **21**, 249–261; Brockmann (1981) Ph.D. Thesis, University of Minnesota; Rebours *et al.* (1992) *J. Aerosol. Sci.* **23**, S189–S192; Stolzenburg (1988) Ph.D. thesis, University of Minnesota) has shown that for particles smaller than about 15 nm, pulse heights produced by the optical detector in a white-light ultrafine condensation nucleus counter (UCNC; Stolzenburg and McMurry (1991) *Aerosol. Sci. Technol.* **14**, 48–65) decrease with initial particle size. We have previously reported on the use of pulse heights from this instrument to determine the concentrations of freshly nucleated atmospheric nanoparticles in the 3–4 nm diameter range (Weber *et al.* (1995) *J. Atm. Sci.* **52**, 2242–2257; Weber *et al.* (1997) *J. Geophys. Res.* **102**, 4375–4385). In this paper we report on the inversion of measured pulse-height distributions to obtain size distributions of particles in the 3–10 nm diameter range. Using methods developed by Stolzenburg (Stolzenburg (1988) Ph.D. Thesis, University of Minnesota) the effect of diffusional broadening is taken into account so as to obtain monodisperse kernel functions from measured pulse-height distributions produced by DMA-generated calibration aerosols in the 3–50 nm diameter range. These kernel functions are then used with the MICRON algorithm described by Wolfenbarger and Seinfeld (1990, *J. Aerosol. Sci.* **21**, 227–247) to obtain size distributions of nanoparticle aerosols from measured pulse height distributions. Calculations were done to ensure that assumed pulse-height data generated from selected known size distributions can be inverted to recover the original size distribution. Results from these validation studies are discussed. Applications of the inversion algorithm to data acquired in studies of homogeneous nucleation in the atmosphere are also presented. Published by Elsevier Science Ltd

BACKGROUND

Steady flow condensation nucleus counters (CNC) are used extensively to measure number densities of atmospheric particles too small to be detected optically. In these instruments particles are grown to light-scattering sizes by exposure to a supersaturated vapor, typically alcohol. Supersaturation is achieved by saturating the aerosol at an elevated temperature then cooling it in a condenser. Particles traversing the condenser increase in diameter by orders of magnitude reaching light-scattering sizes by the time they enter the optical detection cell following the condenser. There, light scattered by individual particles is measured by a photodetector and recorded as a voltage pulse. Earlier investigators observed that in certain CNC's photodetector pulse heights increase with initial particle size for particles smaller than ~ 10 nm (Ahn and Liu, 1990; Brockmann, 1981; Rebours *et al.*, 1992; Stolzenburg, 1988).

The observed dependence of pulse height on initial particle size occurs because small particles grow to a smaller final droplet size in the condenser than do larger ones. This is because the supersaturation that is required to activate condensational growth increases as droplet sizes decrease. Saturation ratios increase from a value of 1.0 near the condenser inlet

[†]Author to whom correspondence should be addressed.

to a maximum in the midsection. Therefore, small particles must travel farther into the condenser before they are exposed to a sufficiently high saturation ratio to initiate condensational growth. Because they have a shorter time to grow before reaching the optical detector, they grow to a smaller final size and scatter less light. Particles activated near the entrance to the condenser reach similar final sizes and produce similar pulse heights.

In the ultrafine condensation nucleus counter (UCNC) of Stolzenburg and McMurry (1991) aerosol is constrained by the sheath flow to the centerline of the condenser. All particles experience nearly the same variation of saturation ratio, which peaks near 4 about halfway through the condenser. Data showing the relationship between pulse height and initial particle diameter for the UCNC is shown in Fig. 1. These results show that for this instrument, particles larger than about 10 nm all grow to similar final sizes and provide no information on initial particle size. However, for smaller particles, Fig. 1 shows that pulse heights could be used to measure number size distributions of particles in the 3–10 nm diameter range. We refer to this as the pulse height analysis (PHA) technique.

Appropriate optics is required to achieve a monotonic relationship between pulse heights and initial particle size. Our UCNC utilizes white light illumination and a detector situated to measure forward scattering (Stolzenburg and McMurry, 1991), such as is used in the TSI 3020 (TSI Inc, St. Paul MN). The TSI 3025 UCNC, which in other respects is similar to the instrument described by Stolzenburg and McMurry (1991), employs a laser light source and a detector located 90° to the incident beam. Mie resonance's from the monochromatic illumination lead to a non-monotonic relationship between pulse height and size (Marti *et al.*, 1996). An alternative PHA system that involves the use of an optical counter to measure pulse-height distributions for particles in the 4–20 nm diameter range was described by Rebours *et al.* (1996).

We have experimentally studied the PHA technique (Saros *et al.*, 1996) to understand what parameters influence UCNC pulse heights. Because growth in the condenser determines the final particle size, factors which alter the saturation profiles will affect pulse heights. Saturation profiles are determined by rates of heat and mass transfer to the condenser walls, and therefore depend on CNC operating parameters and ambient pressure. Saros *et al.* (1996) studied the effect of pressure on nanoparticle pulse heights for pressures down to 0.25 atm. They found that pulse heights are affected by pressure, but that the pulse-height difference for particles of different size was independent of pressure. This simplifies data analysis when the PHA technique is used in aircraft. Particle concentrations can also influence pulse-heights through vapor depletion and coincidence counting. Considering only the peaks in the pulse-height distributions, Saros *et al.* (1996) concluded that pulse-height differencing removes changes due to vapor depletion. The effect of particle coincidence on pulse heights was found to be insignificant if measurements were done at concentrations less than $\sim 4000 \text{ cm}^{-3}$. Finally, the influence of particle composition on pulse heights was also studied. For the materials tested, no dependence was observed.

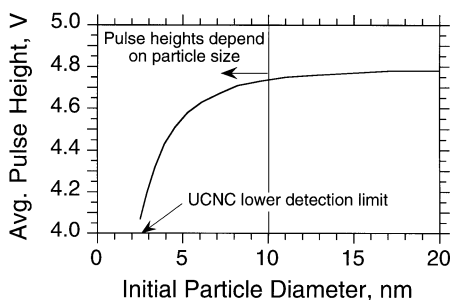


Fig. 1. Average voltage pulse-height from the photodetector of a white light ultrafine particle condensation nucleus counter (UCNC) versus initial particle size. Pulse-heights from particles smaller than approximately 10 nm depend on the initial particle size.

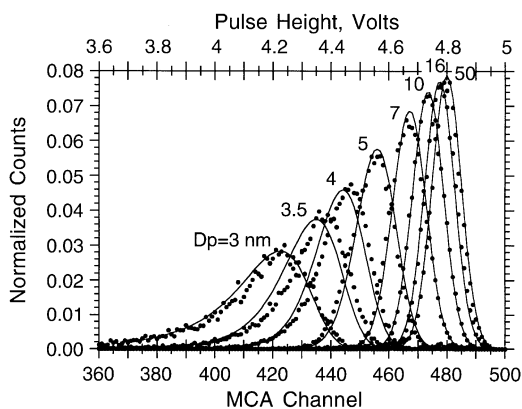


Fig. 2. Kernel functions at 0.67 atm using $(\text{NH}_4)_2\text{SO}_4$ calibration aerosols of several sizes. Pulse-height distributions were measured with a multi-channel analyzer (MCA). The data points show raw data. The solid lines show the “true monodisperse” kernel functions from equation (A1), obtained by deconvoluting the data to account for the range of particle sizes at the exit from the DMA. Note that the measured and “true monodisperse” kernel functions are similar, indicating that the effect of size dispersion of the laboratory-generated calibration aerosols is negligible.

Pulse-height distributions produced by monodisperse ammonium sulfate aerosols of various sizes are shown in Fig. 2. A differential mobility analyzer (DMA) (Knutson and Whitby, 1975) was used to produce the calibration aerosols. Since the aerosol was not neutralized prior to sampling with the UCNC, the calibration particles were charged. This is not expected to influence particle activation and thus pulse heights. A multi-channel analyzer (EG&G Ortec ACE-2K Spectrum Master Model 916) was used to measure pulse-height distributions produced by the UCNC photodetector. Details of the experimental procedure are discussed by Saros *et al.* (1996). In our earlier studies of atmospheric new particle formation and nanoparticle growth (Weber *et al.*, 1995, 1996, 1997) we used the number of counts in channels below 420 to estimate the concentration of particles in the 3–4 nm (nominal) diameter range (see Fig. 2). Channel 420 was chosen so that only particles near the lower detection limit of the UCNC were considered. Although this approach accounts for less than 50% of the detected 3–4 nm particles, (see Fig. 2), its ability to measure very low concentrations of 3–4 nm particles and to clearly distinguish particles near the lower detection limit of the UCNC from larger particles have proven invaluable. While straightforward to implement, the approach uses only a small fraction of the information on particle size provided by the pulse-height measurements.

This paper discusses our work to invert pulse-height distributions to obtain nanoparticle size distributions. We first derive analytical expressions for monodisperse kernel functions from the experimental data. This kernel is then used in the inversion algorithm, MICRON (Wolfenbarger and Seinfeld, 1990), to convert measured pulse-height distributions to number size distributions for particles with diameters between 3 and ~ 10 nm. Numerical studies are used to gauge the quality of the inversion and examples of nanoparticle size distributions derived from pulse-height measurements in the remote troposphere are also presented. Limitations of the technique are discussed.

THEORY

The relationship between measured pulse-height distributions recorded with a multi-channel analyzer and the aerosol size distribution $n(D_p)$ is

$$R_i = \int_0^{\infty} K_i(D_p) dD_p + \varepsilon_i, \quad (1)$$

where R_i is the number of pulses falling within the voltage range assigned to MCA channel i , $K_i(D_p)$ is the probability that a particle of size D_p is assigned to channel i (also referred to as

the “kernel function”), $n(D_p)dD_p$ is the number of particles between D_p and $D_p + dD_p$, and ε_i is the measurement error. Each measured pulse-height distribution provides a set of integral equations that must be solved (“inverted”) for the aerosol size distribution function, $n(D_p)$. More than one distribution function can typically be found that agrees with data to within experimental error, so inversion algorithms usually impose constraints on the distribution function in order to obtain a result.

It is well known that near the detection limit, UCNC counting efficiencies decrease with decreasing particle size (Porstendörfer and Soderholm, 1978; Stolzenburg and McMurry, 1991; etc.). Therefore, for the inversion to predict the true size-distribution sampled by the UCNC, the counting efficiencies for particles must be incorporated with the kernel functions, K_i . Alternatively, by not including the counting efficiency, the kernel functions will apply only to particles that are detected. The inverted size distribution, $n(D_p)$, is then the distribution of the detected particles. The true size distribution of the sampled aerosol can be calculated from the detected distribution by dividing by the UCNC counting efficiency. In the present study we have chosen not to include counting efficiencies in the inversions or to apply the counting efficiency to the inverted size distributions. Our rationale for not including counting efficiencies is that as particle size decreases, efficiencies approach zero and are not accurately known. Furthermore, efficiencies depend on pressure, and we have not investigated this dependence with sufficient care to justify including them in the analysis. Because efficiencies are small and highly uncertain for particles smaller than ~ 3 nm, including them would lead to large uncertainties in the inverted size distributions. For example, Stolzenburg and McMurry (1991) report a UCNC counting efficiency for 3 nm particles in the range of 50–70%, whereas Wiedensohler *et al.* (1997) measured 3 nm efficiencies ranging from ~ 70 to 100%. By not including the counting efficiency, the resulting distribution of detected particles, $n(D_p)$, provides a clear lower limit to the actual distribution sampled.

We also assume that no particles smaller than 2.5 nm produce detectable pulses. Stolzenburg and McMurry (1991) reported that the smallest detectable particle size for our instrument at atmospheric pressure is ~ 2.6 nm. Thus, our chosen lower limit is in reasonable agreement with this value. It must be emphasized that due to uncertainties in K_i and counting efficiencies for particles smaller than 3 nm, inverted distributions below this size are highly uncertain.

Monodisperse kernel functions

Use of accurate kernel functions, $K_i(D_p)$, is an essential component of inversion. The data in Fig. 2 provide reasonable estimates of kernel functions for 8 particle sizes between 3 and 50 nm. From our previous work (Stolzenburg, 1988), however, we know that particles produced by the DMA are not perfectly monodisperse. Instead, they cover a range of sizes which increases, due to diffusion, as particle size decreases. In an attempt to correct for this, a deconvolution of the experimental data was undertaken to generate monodisperse kernels. Analytical expressions for the kernels were fit to the experimental data using essentially a least-squares method. The resulting fitted kernels give smooth pulse-height distributions for monodisperse particles as well as a smooth dependence of pulse-heights on particle size. Compared to inversions with kernels comprised of experimental data, an added benefit of fitting and deconvolution is that the acquired analytical kernel functions improve the inversion accuracy and efficiency by eliminating interpolation between noisy experimental data.

The experimental data to which the kernel functions were fit consisted of measured pulse-height distributions for DMA-derived aerosols at 13 particle sizes between 3 and 16 nm and one more at 50 nm representing the size-independent response of “large” particles. A subset of these data is shown in Fig. 2. The analytical form of the monodisperse kernel function, $K_i(D_p)$, was fit to these data through equation (1), where R_i represents the measured pulse-height distributions and $n(D_p)$ is the aerosol distribution exiting the DMA. In this case, equation (1) was normalized by dividing by the total particle count. R_i becomes

the fraction of pulses falling in channel i and $n(D_p)$ becomes essentially the DMA transfer function. The transfer functions were obtained in theoretical analytical form from the work of Stolzenburg (1988) accounting for the diffusional broadening in the DMA. The choice of the parameterized analytical form of the kernel function is discussed below. The integrals were calculated numerically. The fit was obtained by minimizing the weighted sum of squares of relative differences between the fitted and smoothed measured normalized responses, R_i , in 21 selected channels for each of the 14 pulse-height distributions. The selected channels for each pulse-height distribution included the peak channel and channels on either side of the peak at about 0.9, 0.8, ..., 0.1 and 0.05 times the peak height. The number of channels used in the fit was limited due to the computation effort required for numerical integration and the measured data were smoothed to reduce Poisson noise. The data at 3 and 3.5 nm and at 50 nm were weighted more heavily because of their importance in extrapolating down to 2.5 nm and as the “large” particle reference, respectively. A variety of techniques were used to minimize the residuals, including gradient search and the simplex method (Nelder and Mead, 1965).

No calibration data were obtained below 3 nm because of the difficulties in producing aerosols that small. However, the kernels used during inversions must be extrapolated down to 2.5 nm, as noted below. For extrapolation, a single parameterized functional form for $K_i(D_p)$ was sought with relatively few degrees of freedom. By comparing the overlap of DMA transfer functions including diffusion at adjacent sizes, such as 3 and 3.5 nm, to the much greater overlap of their corresponding pulse-height distributions (Fig. 2) it was apparent that most of the dispersion in the measured pulse-height distributions is inherent to the UCNC, and not due to the finite dispersion of particle sizes exiting the DMA. This was true even at the smallest size (3 nm) where most diffusional broadening of the DMA transfer function occurs. Thus, the raw data, as in Fig. 2, are very close to the monodisperse kernel function being sought and a parameterized functional form which fits the former should also fit the latter with relatively small parameter adjustments. The dependence of $K_i(D_p)$ on channel number, i , has the appearance of a skewed normal distribution which is fit quite well by the form given in equation (A1) in Appendix A, where the parameters B , C and D are fixed for a given diameter D_p . Forms to fit the diameter dependence of these three parameters were then found as shown in equation (A2). This functional form of the kernel was first fit directly to the experimental data without convoluting $K_i(D_p)$ with the DMA transfer function using equation (1). The resulting set of fitted parameters was then used as a starting point for the minimization procedure using equation (1) as described above. The final set of 12 fitted parameters is also shown in Appendix A.

Figure 2 shows the final fitted monodisperse kernel functions at the same diameters as the corresponding raw data for the DMA aerosols. They fit very closely indicating that the effect of the finite dispersion of the DMA aerosols is nearly negligible. Most of the offset in channels between the monodisperse kernels and the raw data apparent at 3.5 and 4 nm is due to residuals in the diameter dependence fits represented by equation (A2). Thus, constraining the kernel function by these analytical forms has introduced a small amount of bias in the fitted kernel. Some of this “bias” might actually be caused by skewing of the measured responses due to the shape of the DMA input distribution and the diameter dependence of the UCNC counting efficiency. These effects could only be partially accounted for in the fitting process.

The inversion algorithm

A variety of algorithms have been reported for inverting aerosol measurements to obtain size distributions. They include the iterative method of Twomey (1975), the expectation maximization method of Maher and Laird (1986), the lognormal simplex method of Reineking and Porstendörfer (1986), the extreme value estimation (EVE) of Paatero (1990), and the constrained regularization approach of Wolfenbarger and Seinfeld (1990). The Twomey and expectation maximization methods discretize the size distribution yielding linear equations which can be solved by iteration. The lognormal simplex method assumes,

a priori, lognormal size distributions. Paatero's approach provides a set of solutions for $n(D_p)$ that is consistent with data to within the specified measurement uncertainty. Wolfenbarger and Seinfeld's method (MICRON) using constrained regularization and generalized cross validation predicts a most probable distribution by recognizing that errors associated with the data are not independent and constraining the solution to smooth non-zero distributions. This specific approach is referred to here as MICRON. We have chosen to use MICRON to convert UCNC pulse-height measurements to particle size distributions because of its flexibility. Many of the other inversion techniques were developed for different aerosol inversion problems.

To invert observed pulse-height distributions, the inversion problem is to find a smooth size distribution, $n(D_p)$, that agrees with the measured pulse-height data. In MICRON this is achieved by minimizing, subject to constraints, the function,

$$\sum_i \left[\frac{\int_0^\infty K_i(D_p)n(D_p)dD_p - R_i}{E_i} \right]^2 + \lambda \int_0^\infty \left(\frac{d^2n(D_p)}{dD_p^2} \right)^2 dD_p, \quad (2)$$

where E_i is our estimate of the measurement error, ε_i . The first part of this function considers the difference between the predicted and observed data and the second part gives a measure of the degree of smoothness of the predicted size distribution. The importance given to smoothness in the inverted data is determined by the regularization parameter, λ . The solution depends on the value of λ used. If λ is too large the data will be undervalued and the solution over-smoothed. Too small a value will excessively weight the data and solutions may contain nonexistent structure resulting from errors in the data. MICRON chooses an appropriate λ by generalized cross validation. These techniques are employed by MICRON to obtain a single solution to the general inversion problem.

To invert UCNC pulse height distributions we seek solutions over a wide size range 2.5–1000 nm, since the measured pulse-height distributions contain pulses from all particles with diameters larger than roughly 2.6 nm. The upper size limit is arbitrary, provided that it is considerably greater than ~ 10 nm. The resulting size distributions for particles larger than roughly 10 nm are ignored since pulse heights provide no size information for larger particles.

The pulse height data for inversion consists of the number of counts and its associated error (E) for channels 375–499 (see Fig. 2). The error was calculated, assuming Poisson counting statistics, as the square root of the response. For channels where the response was zero, the error was assigned a value of 1. This afforded the inversion some freedom even in channels in which no counts were recorded.

RESULTS

Numerical test of inversions

Numerical experiments were performed as one way of evaluating the quality of the size distributions generated by MICRON. We assumed that the distribution of detected particles, $n(D_p)$, was lognormal and calculate the expected pulse-height distributions, R_i , from equation (1), adding random noise. This was a blind test since the pulse-height distributions were generated independently of MICRON.

Since the goal was to ultimately invert atmospheric data, the assumed distributions always included particles larger than 10 nm at levels typical of those encountered in the remote troposphere. The shape of this larger particle mode did not influence the pulse height distribution or inversion since, at these sizes, all particles produce similar pulse heights. In all tests, the larger size mode was lognormal with a typical number concentration of 400 particles cm^{-3} . Numerical experiments were performed for a wide variety of assumed unimodal and bimodal nanoparticle distributions. Tests included distributions with number median diameters between 2.5 and 15 nm, geometric standard deviations of 1.2–1.6, and concentrations of 0–1000 particles cm^{-3} . Three numerical tests are discussed here.

Figure 3a shows an assumed distribution consisting of a bimodal lognormal nanoparticle mode with peaks at 3.5 and 7 nm and the larger fine particle mode. The “measured” pulse-height distribution, calculated from the distribution shown in Fig. 3a, with added noise, is shown in Fig. 3b. The noise was calculated as 10% of the response at that channel times a random number between -1 and 1 . This pulse-height distribution is inverted by MICRON to obtain the measured size distribution. The inversion result and original assumed distribution are shown in Fig. 3c. The inversion agrees remarkably well with the original distribution for sizes between approximately 2.5 and 10 nm. For particles larger than 10 nm, the inversion deviates from the assumed distribution. This is expected since at these sizes the pulse-height distributions provide no information on size (e.g., see Figs 1 and 2). Figure 4 shows a distribution that might be found if nucleation were occurring. In Fig. 5, the assumed distribution peaks above 10 nm but tails off into the nanoparticle size range where the PHA technique provides some size information. In both cases the inversions agree well for sizes between 3 and 10 nm.

These numerical experiments suggest that MICRON can accurately convert pulse-height distributions to size distributions for particles between approximately 3 and 10 nm. However, these tests are somewhat circular in nature. For example, both the generated pulse-height distribution and the inversion use the same kernel functions. In practice, during a particular measurement, kernel functions may change. To further test the inversions, atmospheric pulse-height distributions are inverted and the resulting size distributions compared to related but independent aerosol measurements.

Inversions of atmospheric measurements

We have completed ground-based studies of new particle formation and nanoparticle growth in the remote troposphere at the Mauna Loa Observatory, Hawaii, 1992, and Idaho

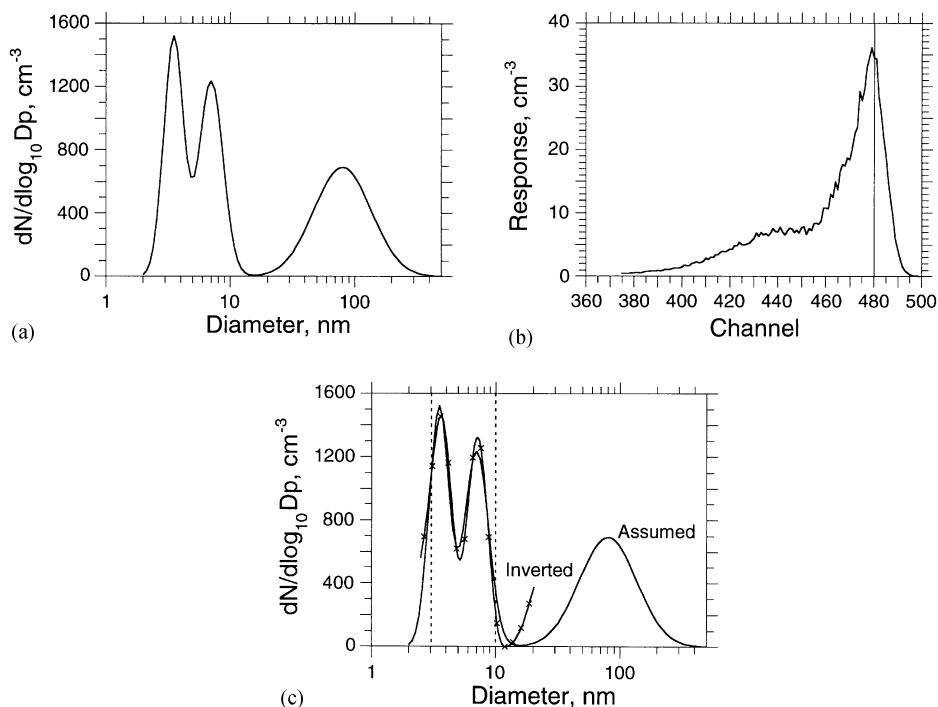


Fig. 3. Results of a numerical experiment. The assumed multi-modal lognormal distribution (a) was used to calculate the pulse-height distribution in (b) which includes added random noise. This calculated pulse-height distribution is inverted to obtain a size distribution which is compared with the assumed distribution in (c). The inverted results agree in the size range 3–10 nm where pulse-heights are dependent on particle size.

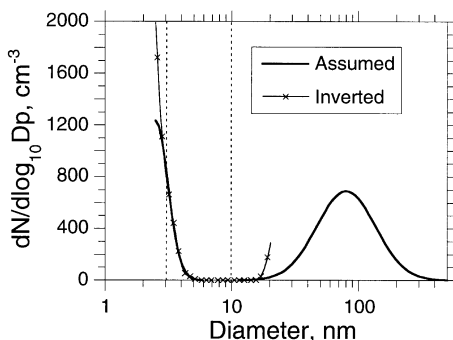


Fig. 4. Results of a numerical experiment with an assumed distribution that may be found in regions of new particle formation. The inversion recovered the assumed nanoparticle distribution.

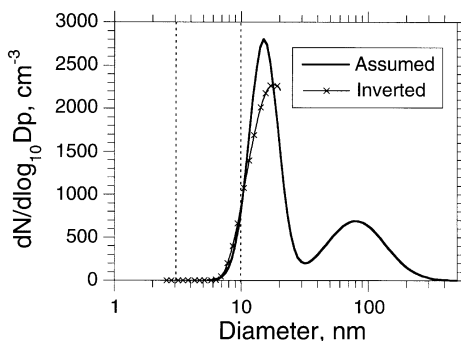


Fig. 5. Results of a numerical experiment with an assumed lognormal nanoparticle distribution with count median diameter of 15 nm. The inverted results agree well with the original assumed distribution for particle sizes up to approximately 10 nm.

Hill, Colorado, 1993. Similar measurements were made in both studies. The UCNC-PHA system was used to measure the total and nanoparticle concentrations (3–10 nm) and a scanning mobility spectrometer (Wang and Flagan, 1990) was used to measure sizes of particles between approximately 20 and 500 nm diameter. Although the two instruments do not measure concentrations of overlapping particle sizes, comparing the size distributions can provide some insight into the quality of the PHA derived nanoparticle size distribution.

Figure 6 shows the UCNC-PHA and SMPS size distributions measured on July 15, 1992 at the Mauna Loa Observatory. Both the UCNC-PHA and SMPS measurements indicate growth of nanoparticles as the morning progressed. For Figs 6a–c, the PHA data shows an increase in the diameter associated with the peak of the nanoparticle mode. Changing with time, these diameters are 5.6, 7.5 and 9 nm, respectively. This movement to larger sizes slowly closes the gap between the nanoparticle and fine modes. By afternoon the nanoparticles have almost completely grown out of the range that can be resolved by the UCNC-PHA and into the range measured by the SMPS. Overall, the values of the distribution obtained at the large end of the UCNC-PHA range appear to be reasonably consistent with distributions at the small end of the SMPS range.

The PHA technique was also deployed on an aircraft. We participated in the Southern Hemisphere Marine Aerosol Characterization Experiment (ACE-1), 31 October–22 December 1995, to study nucleation in the remote South Pacific. Particularly intriguing data were acquired during one flight in which measurements were made downwind of large penguin colonies on Macquarie Island (54.5°S, 159.0°W). No nano-size particles were detected in air free of island influence. Downwind of colonies, however, the pulse-height data showed dramatic evidence of new particle formation and subsequent particle growth. Figure 7 shows the evolution of the PHA derived nanoparticle distribution as air was transported

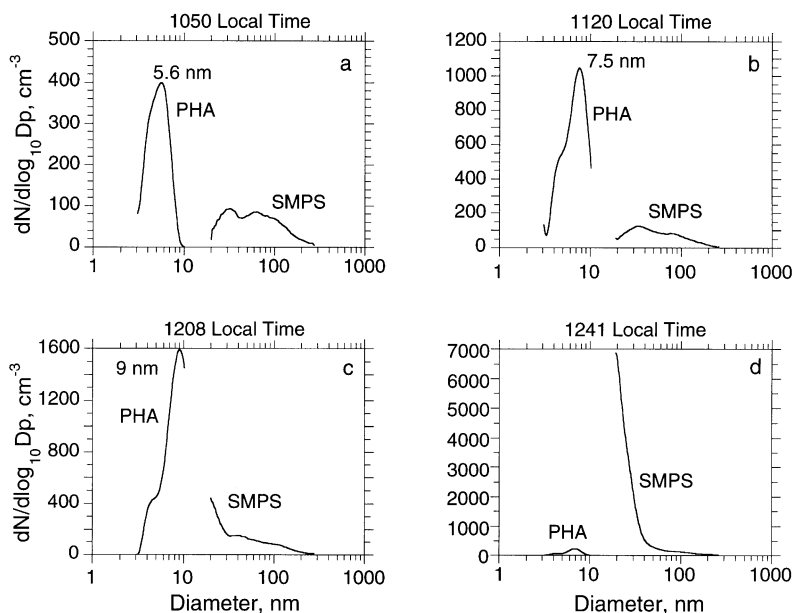


Fig. 6. Nanoparticle and fine particle size distributions measured by UCNC pulse-height analysis (PHA) and a scanning mobility particle spectrometer (SMPS), respectively, at the Mauna Loa Observatory, 15 July 1992. The sequence (a), (b), (c) and (d) shows the growth of the nanoparticle mode to larger sizes from mid-morning to afternoon. The SMPS measurements are consistent with the UCNC-PHA distributions providing some confidence in the measurement of nanoparticle distributions by pulse-height analysis.

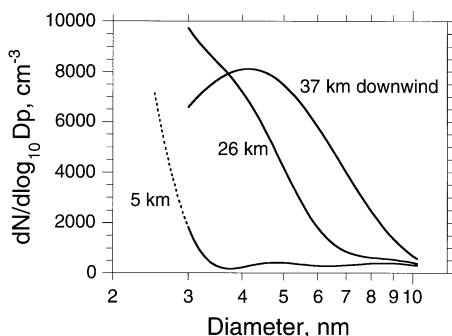


Fig. 7. Nanoparticle size distributions, measured by UCNC pulse-height analysis (PHA) downwind of a large penguin colony on the coast of Macquarie Island (54.5°S , 159.0°W). The three distributions were measured downwind from the colony at average distances of ~ 5 , 26, and 37 km. The distributions show evidence of new particle formation and subsequent growth of the newly formed particles to larger sizes.

away from a large penguin colony near the northern tip of Macquarie Island. Close to the colony, ~ 5 km downwind, the high concentrations of the smallest detectable particles suggest that they were newly formed by nucleation of gases, some of which were probably of biogenic origin.* As distance downwind of the colony increased, we detected large numbers of particles at increasingly larger sizes, indicating growth of the newly formed particles.

When coupled with simultaneous measurements of condensable gas phase species, these nanoparticle size distributions can provide new insights into the microphysics of new particle formation and nanoparticle growth.

*In this case we have plotted the distribution down to 2.5 nm. However, the results below 3 nm are highly uncertain since UCNC efficiency drops off rapidly to zero in this range and was not considered in the inversion. In any case, for the measurement close to the island, the inversion indicates that most of the nanoparticles detected were near the lower detection limit of the UCNC.

DISCUSSION

For the range of conditions tested in our numerical experiments, we have found that for particles between 3 and 10 nm diameter, inversion by MICRON recovers the assumed size distribution. We have also found that ambient nanoparticle distributions derived from UCNC-PHA measurements were consistent with other measurement techniques. However, we have also observed that there are instances when inversion of ambient data can be problematic. These difficulties occur when there are differences between the actual kernel functions which existed at the time of the pulse-height measurements, and the kernel functions used for the inversion, which are assumed to be invariant.

Conditions encountered during atmospheric measurements can influence kernel functions. For example variations in pressure or UCNC temperatures during the acquisition of a pulse-height distribution would lead to broadened kernel functions. Analysis of the ambient data has also pointed to high particle concentration as a cause for inversion difficulties. In light of this, the earlier experiments of Saros *et al.* (1996) were reanalyzed to see how particle concentration influences the shape of the pulse-height distributions.

Figure 8 shows the kernel function for 50 nm particles (from Fig. 2) and two measured pulse-height distributions for a laboratory generated aerosol consisting of monodisperse 3 and 50 nm diameter sodium chloride particles.[†] For comparison, each mode has been normalized separately. Because pulse-heights decrease with increasing particle concentration (Saros *et al.*, 1996), the distributions were translated so that the mean channel of the larger mode equaled 480. In these experiments the concentration of the 50 nm particles was varied while the concentration of the 3 nm particles was kept fairly constant at 200–300 cm⁻³. The results show that for higher 50 nm-particle concentrations, the normalized pulse-height distributions for 50 nm particles are broader, but the pulse-height distributions for 3 nm particles are only weakly affected. No other sizes of nanoparticles were tested, thus the effect of fine mode concentrations on other nanoparticle pulse-height distributions is not known. Neither did we investigate the sensitivity of kernel functions to nanoparticle concentrations. Note from Fig. 8 that the 50 nm kernel used in the inversions and the pulse-height distribution for a concentration of 490 cm⁻³ are similar. This is because the kernel functions shown in Fig. 2 were obtained using concentrations between approximately 500 to 600 cm⁻³.

By fitting the 50 nm-particle pulse-height distribution with a Gaussian distribution, the standard deviation was calculated and used as a measure of the concentration-dependent broadening. A similar calculation was not done for the 3-nm pulse-height distribution since it is skewed and only weakly dependent on fine mode concentrations. Figure 9 shows that the standard deviation for the “large” particle kernels increases linearly with “large” particle concentration. We believe this is due to the stochastic nature in which vapor depletion and latent heat effects influence droplet growth. The effect of these processes on droplet growth depends on the distance between the drop and its nearest neighbor. This distance is smaller at higher concentrations and is a random variable with a probability distribution. A simple analysis suggests that these stochastic processes can account for the observed linear increase in breadth of the pulse-height distribution with increasing droplet concentration.

To investigate the sensitivity of inverted ambient distributions to kernel broadening, more numerical experiments were performed. In these experiments, pulse-height distributions that would be obtained from assumed size distributions were calculated by making a range of assumptions about the kernel functions. In all cases we assumed that the kernel functions for 3–10 nm particles are unaffected by concentration, since this is in reasonable agreement with the available laboratory data (Saros *et al.*, 1996). However, the concentration-dependent kernel functions for 50 nm particles shown in Figs 8 and 9 were used to

[†]Note that compared to the kernel function for 3 nm particles in Fig. 2, pulse-heights for 3 nm NaCl particles in Fig. 8 are smaller. This is discussed in Saros *et al.* (1996) where it was concluded that differences were due to DMA classification of cubic NaCl particles.

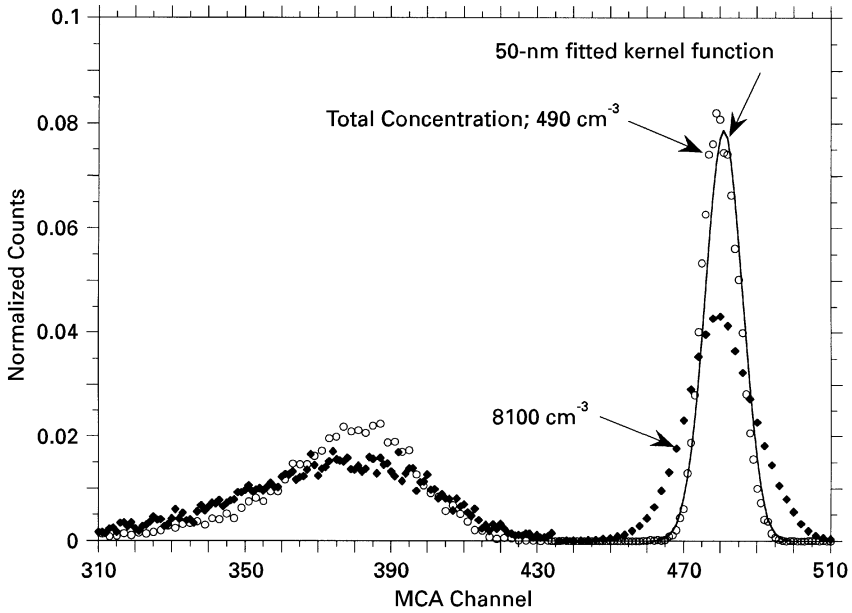


Fig. 8. Results of earlier laboratory studies (Saros *et al.*, 1996) where aerosols consisting of monodisperse 3 and 50 nm NaCl particles were generated to study the effect of particle concentration on pulse-heights. UCNC pulse-height distributions are compared for total particle concentrations of 490 and 8100 particles cm^{-3} . For comparison, the 3 nm modes were normalized over channels 300–439 and the 50 nm modes were normalized over channels 440–520. The distributions show that higher particle concentrations result in broader pulse-height distributions. The effect is most pronounced for larger pulse-heights. The kernel function for 50 nm particles used in the inversion is also shown.

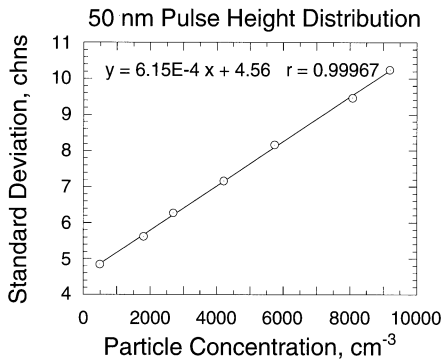


Fig. 9. Broadening of UCNC pulse-height distributions for 50 nm particles due to particle concentration. Normalized pulse-height distributions were fitted by Gaussian distributions to obtain the standard deviation. The breadth of the distributions, given by the standard deviation, increases linearly with total particle concentration even at low concentrations.

obtain a range of pulse-height distributions for “large” particles. The calculated pulse-height distributions were then inverted by MICRON using the kernel functions applicable to low concentrations of “large” particles shown in Fig. 2.

Figure 10 shows the relationship between assumed and calculated distributions for an aerosol that consists of nanoparticle modes peaking at 3 and 7.5 nm, each containing 100 particles cm^{-3} . The concentration of “large” particles was varied from 600–3000 cm^{-3} . Note that in this case the spreading of the “large” particle pulse-height distribution adversely influenced the inverted 3–10 nm size distributions for concentrations of “large” particles equal to or greater than $\sim 2000 \text{ cm}^{-3}$.

We expect broadened kernels to cause the most problems when concentrations of 3–10 nm particles are very low. This is because in these cases the nanoparticle pulse-height

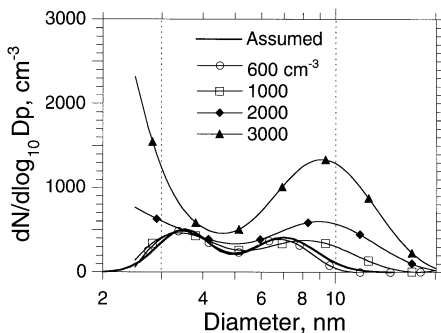


Fig. 10. Results of a numerical experiment testing the influence of kernel broadening due to particle concentration on inverted size distributions. Pulse-height distributions were generated from an assumed size distribution with modes at 3.5 and 7 nm, each containing concentrations of 100 cm^{-3} . Concentrations of “large” particles were varied from $600\text{--}3000 \text{ cm}^{-3}$. Concentration-dependent kernel functions from Fig. 9 were used to generate the pulse-height distributions. These distributions were inverted with the fitted kernel functions (see Fig. 2) which do not consider the effect of concentration. Note that significant errors occur for concentrations greater than $\sim 2000 \text{ cm}^{-3}$.

distribution will be dominated by pulses from particles larger than $\sim 10 \text{ nm}$ due to their broader kernel functions. To test this, two particle distributions were assumed. One consisted of a nanoparticle and a fine particle mode, each containing 500 cm^{-3} . The other distribution had no nanoparticle mode but retained the same fine-particle mode. A broadened kernel function for the “large” particles with a standard deviation of 9.5 channels was used to generate the pulse-height distributions. These pulse-height distributions were inverted with the fitted kernels used for inverting ambient data, and which are considered invariant. The resulting nanoparticle distributions are shown in Fig. 11 along with the assumed distributions. Figure 11 shows that the broadened kernel function has much less influence on the inversion if the measurement contains significant numbers of nanoparticles. For the results shown in Fig. 11a, the broadened kernel results in a small mode between 6 and 10 nm; we have seen evidence for this artifact when inverting ambient data with high concentrations of “large” particles. In this case useful information about nanoparticle distributions, particularly towards the lower detection limit of the instrument, is still obtained. However, the results in Fig. 11b show that if the distribution contains no pulses from nanoparticles, the broadened large-particle kernel leads to a significant overestimate of nanoparticle concentrations. When inverting ambient data this error is easily identified by comparing the total concentration of the inverted distribution with the total measured concentration. Large discrepancies point to poor inversions. For example, for Figs 11a–b, the errors in total concentrations are 12 and 560%, respectively. The examples of inverted atmospheric pulse-height distributions shown in Figs 6 and 7 were not greatly influenced by pulse-height spreading since in these cases the total aerosol concentrations were either low or there were large numbers of nanoparticles present.

To summarize, inversions of ambient pulse-height distributions are complicated by the fact that kernel functions can depend on sampling conditions. Numerical experiments suggest that the present kernel functions, which do not account for kernel broadening, are limited to situations where concentrations are less than approximately 2000 cm^{-3} . However, broadened kernels for “large” particles have a minor impact on the inversion when the measured size distribution contains significant numbers of nanoparticles relative to the concentration of particles larger than $\sim 10 \text{ nm}$. On the other hand, significant errors can occur when inverting broadened pulse-height distributions that contain few pulses from nanoparticles. Further work to improve our understanding of the causes for changes in kernel functions may permit accounting for these effects when inverting ambient pulse-height data. For example, if the widths of kernel functions could be estimated from the pulses above channel 480, it might be possible to adjust the kernels so that they better match those that existed at the time of the measurement. It should be noted that although

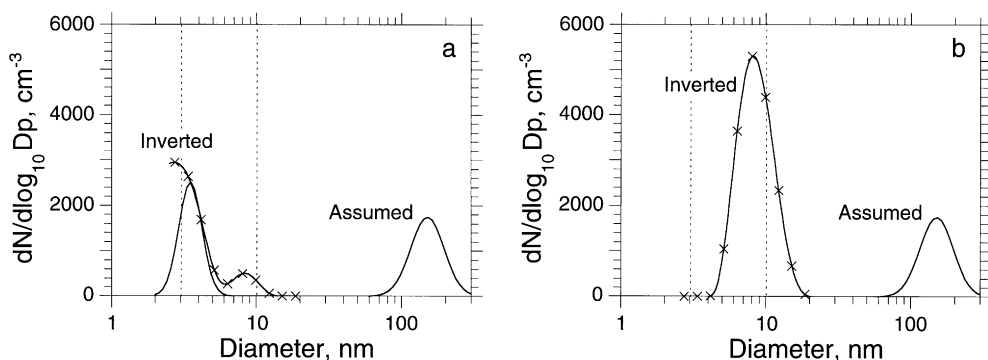


Fig. 11. Results of a numerical experiment showing the effect of kernel broadening on inverted nanoparticle size distributions. Two distributions were simulated. The first, (a), consisted of a nano- and fine particle mode, each containing $500 \text{ particles cm}^{-3}$; the second, (b), retained the fine particle mode (i.e., the “large” particles) but did not include nanoparticles. Pulse-height distributions were generated using the usual fitted kernels (see Fig. 2 and Appendix A), except that a kernel function having a standard deviation of 9.5 channels was used for the “large” particles. These pulse-height distributions were then inverted with the fitted kernels that we normally use to invert ambient data (Fig. 2). When nanoparticles are present, the broadened “large” particle kernel has a minor effect. However, significant errors occur for measured distributions which contain few nanoparticles.

broadening of the pulse-height kernels can adversely influence the inverted 3–10 nm size distributions, it has only a minor influence on the simple approach of estimating concentrations of nominally 3–4 nm particles used in our earlier work (Weber *et al.*, 1995, 1997). For this calculation, only pulses smaller than channel 420 are counted. The data in Fig. 8 show that the “large” particles do not contribute to counts in this range even at high concentrations where kernels are significantly broadened.

CONCLUSIONS

We have presented results which suggest that UCNC photodetector pulse-height distributions can be inverted by constrained regularization and generalized cross validation to obtain size distributions of particles between 3 and 10 nm diameter. We used the algorithm MICRON described by Wolfenbarger and Seinfeld (1990) to carry out these inversions. Particular care was taken to generate accurate monodisperse kernel functions used in the inversion. Both numerical experiments and atmospheric data support the plausibility of the PHA inversion results. In some cases, inversion of ambient pulse-height distributions can be troublesome due to differences between the ambient kernel functions and the laboratory-derived kernels used for the inversion. Further work to characterize the effect of parameters which influence pulse heights may permit compensating for their influence when inverting ambient data.

Other approaches exist for measuring nanoparticle size distributions, such as size classification with a DMA (Chen *et al.*, 1997). The size resolution obtained by the DMA is superior to that from the PHA technique, but the PHA technique offers the advantage that size distributions can be measured more quickly. This is advantageous for remote atmospheric measurements where concentrations can be exceedingly low (total concentrations of $\sim 200 \text{ cm}^{-3}$, nanoparticle concentrations less than $\sim 0.1 \text{ cm}^{-3}$) or for airborne measurements where fast measurements are essential. For example, only $\sim 1\%$ of the 3 nm particles are charged, so the time required to count a statistically significant sample downstream of a DMA at this size is ~ 100 times greater than is achieved with the PHA technique. Furthermore, the PHA technique sizes all particles simultaneously, while the DMA measures each size individually.

Overall, the fundamental strength of the PHA technique is that it is the only method currently available which sizes all nanoparticles simultaneously. This technique provides a substantial amount of information on nanoparticle spectra. Measured

pulse-height distributions can be inverted by an algorithm like MICRON to obtain 3–10 nm size distributions. Alternatively, by counting only a subset of the total pulses, concentrations of particles in a narrow diameter range (e.g., ~3–4 nm) can be estimated. Moreover, the pulse-height measurements can be done in conjunction with the traditional application of the UCNC. For example, an additional data acquisition system could count pulses at a high rate (e.g., 1 Hz), thereby providing high time resolution of total CN concentrations.

Acknowledgements—We thank Prof. Lynn Russell of Princeton University for her comments and suggestions regarding the MICRON inversions. Research at BNL was performed under the auspices of the U.S. Department of Energy contract DE-AC02-76CH00016 Atmospheric Chemistry Program within the Office of Health and Environmental Research. This work was also supported by Department of Energy Grant No. DE-FG02-91ER61205. By accepting this article, the publisher and/or recipient acknowledges the U.S. Government's right to retain a non-exclusive, royalty-free license in and to any copyright covering this paper.

REFERENCES

- Ahn, K. and Liu, B. (1990) Particle activation and droplet growth processes in condensation nucleus counter-1. Theoretical background. *J. Aerosol Sci.* **21**, 249–261.
- Brockmann, J. E. (1981) Coagulation and deposition of ultrafine aerosols in turbulent pipe flow. Ph.D. Thesis, University of Minnesota.
- Chen, D., Pui, D. Y. H., Hummes, D., Fissan, H., Quant, F. R. and Sem, G. J. (1997) Design and evaluation of a nanometer aerosol differential mobility analyzer (Nano-DMA). this issue.
- Knutson, E. O. and Whitby, K. T. (1975) Aerosol classification by electrical mobility: apparatus, theory, and applications. *J. Aerosol Sci.* **6**, 443–451.
- Maher, E. F. and Laird, N. M. (1985) EM algorithm reconstruction of particle size distributions from diffusion battery data. *J. Aerosol Sci.* **16**, 557–570.
- Marti, J. J., Weber, R. J., Saros, M. T., Vasiliou, J. G. and McMurry, P. H. (1996) Technical Note: Modification of the TSI 3025 condensation particle counter for pulse-height analysis. *Aerosol Sci. Technol.* **25**, 214–218.
- Nelder, J. and Mead, R. (1965) A simplex method for function minimization. *Comp. J.* **7**, 308–313.
- Paatero, P. (1990) The extreme value estimation deconvolution method with applications in aerosol science. Univ. of Helsinki, Report Series in Physics, HU-P-250 1–41.
- Porstendörfer, J. and Soderholm, S. C. (1978) Short communication: particle size dependence of a condensation nuclei counter. *Atmos. Environ.* **12**, 1805–1806.
- Rebours, A., Boulaud, D. and Renoux, A. (1992) Production of monodisperse aerosol by evaporation and condensation of vapor under control process. *J. Aerosol Sci.* **23**, S189–S192.
- Rebours, A., Boulaud, D. and Renoux, A. (1996) Recent advances in nanoparticle size measurement with a particle growth system combined with an optical particle counter—a feasibility study. *J. Aerosol Sci.* **27**, 1227–1241.
- Reineking, A. and Porstendörfer, J. (1986) High volume screen diffusion batteries and α -spectroscopy for measurement of the radon daughter activity size distributions in the environment. *J. Aerosol Sci.* **17**, 873–879.
- Saros, M. T., Weber, R. J., Marti, J. J. and McMurry, P. H. (1996) Ultrafine aerosol measurement using a condensation nucleus counter with pulse-height analysis. *Aerosol Sci. Tech.* **25**, 200–213.
- Stolzenburg, M. R. (1988) An ultrafine aerosol size distribution measuring System. Ph.D. Thesis, University of Minnesota.
- Stolzenburg, M. R. and McMurry, P. H. (1991) An ultrafine aerosol condensation nucleus counter. *Aerosol Sci. Technol.* **14**, 48–65.
- Twomey, S. (1975) Comparison of constrained linear inversion and an iterative nonlinear algorithm applied to the indirect estimation of particle size distributions. *J. Comp. Phys.* **18**, 188–200.
- Wang, S. C. and Flagan, R. C. (1990) Scanning electrical mobility spectrometer. *Aerosol Sci. Technol.* **13**, 230–240.
- Weber, R. J., McMurry, P. H., Eisele, F. L. and Tanner, D. J. (1995) Measurement of expected nucleation precursor species and 3 to 500 nm diameter particles at Mauna Loa Observatory, Hawaii. *J. Atm. Sci.* **52**, 2242–2257.
- Weber, R. J., Marti, J. J., McMurry, P. H., Eisele, F. L., Tanner, D. J. and Jefferson, A. (1996) Measured atmospheric new particle formation rates: implications for nucleation mechanisms. *Chem. Eng. Commun.* **151**, 53–64.
- Weber, R. J., Marti, J. J., McMurry, P. H., Eisele, F. L., Tanner, D. J. and Jefferson, A. (1997) Measurements of new particle formation and ultrafine particle growth rates at a clean continental site. *J. Geophys. Res.* **102**, 4375–4385.
- Wiedensohler, A., Orsini, D., Covert, D. S., Coffmann, D., Cantrell, W., Halvlicek, H., Brechtel, F. G., Russell, L. M., Weber, R. J., Gras, J., Hudson, J. G. and Litchy, H. (1997) Intercomparison study of the size-dependent counting efficiency of 26 condensation particle counters. *Aerosol Sci. Technol.* **27**, 224–242.
- Wolfenbarger, J. K. and Seinfeld, J. H. (1990) Inversion of aerosol size distribution data. *J. Aerosol Sci.* **21**, 227–247.

APPENDIX

Analytical expression for UCNC kernels as a function of particle size and pulse-height (channel)

The probability, K , that a detected particle of size D_p (nm) will be counted in channel i is

$$K_i = \exp \left\{ \frac{i-B}{C} D - \frac{1}{2} \left[\left(\exp \left\{ \frac{i-B}{C} D \right\} - 1 \right) / D \right]^2 \right\} / \left\{ \sqrt{2\pi} C \Phi \left(\frac{1}{|D|} \right) \right\}, \tag{A1}$$

where

$$\begin{aligned} B(D_p) &= B_1 + B_2/(D_p - B_3)^{B_4}, \\ C(D_p) &= C_1 + C_2/(D_p - C_3)^{C_4}, \\ D(D_p) &= D_1 + D_2/(D_p - D_3)^{D_4} \end{aligned} \tag{A2}$$

and $\Phi(u)$ is the cumulative normal probability function and

	1	2	3	4
B	480	-513.410	-0.0231	1.877
C	5.057	16.847	1.777	1.869
D	0.0143	283.349	-0.649	4.822

Note that

$$\sum_i K_i(D_p) \cong \int_i K_i(D_p) di = 1$$

as required by normalization of total probability to 1, since counting efficiency is not included.

The calibration data pulse-height distributions were translated so that the peak of the pulse-height distributions for particles much larger than 10 nm (i.e., particles that produce identical pulse-heights) were located at channel 480. Prior to inversion of a measured pulse-height distribution, all measured pulses were also translated so that the peak of the size-independent pulses were also centered at channel 480. In this way, we attempt to remove all factors, other than particle size, which influence observed pulse-heights.